energies

Article

Analysis and Design of Wireless Power Transfer Systems Applied to Electrical Vehicle Supercapacitor Charge Using Variable-Resistance-Based Method

Yuyu Geng, Tao Wang *, Shiyun Xie and Yi Yang

College of Electrical and Electronic Engineering, Chongqing University of Technology, Chongqing 400054, China
* Correspondence: wangtao20190031@cqut.edu.cn; Tel.: +86-177-8338-2839

Abstract: Supercapacitors (SCs) are widely used as energy storage devices in many practical applications of wireless power transfer. However, the modeling and analysis of a wireless power transfer system are seldom based on SC load; thus, the effects of the charging process on the wireless power transfer system cannot be analyzed clearly. In this paper, a variable-resistance-based method is proposed for the modeling and analysis of the process of constant current charging. First, how to make an SC equivalent in variable resistance is described, and the relationship between SC and variable resistance is considered. Next, the charging process, including charging current, voltage, power and transfer efficiency, is analyzed in detail. Furthermore, the effects of transmitting side voltage and frequency offset on this system are studied, and the optimal design method for an SC-load WPT system is provided on a preliminary basis. Finally, the theoretical derivation and analysis are verified by means of simulations and experiments.

Keywords: wireless power transfer; supercapacitor charging; variable-resistance-based; characteristic analysis

Citation: Geng, Y.; Wang, T.; Xie, S.; Yang, Y. Analysis and Design of Wireless Power Transfer Systems Applied to Electrical Vehicle Supercapacitor Charge Using Variable-Resistance-Based Method. *Energies* **2022**, *15*, 5867. https://doi.org/10.3390/en15165867

Academic Editor: Alon Kuperman

Received: 7 July 2022
Accepted: 9 August 2022
Published: 12 August 2022

1. Introduction

Wireless power transfer (WPT) technology has been developed in recent years as a new technology for electric power transmission. WPT technology avoids direct electrical connection, and, thus, brings many advantages, such as the elimination of sparking and risk of electric shock, safe and convenient charging, and ease of achieving an automatic power supply [1–3]. Due to these obvious advantages, WPT has been widely tested and used in many fields, such as rail transportation vehicles, household appliances, biomedical equipment and other applications. WPT technology is conducive to reducing energy storage devices and extending mileage for practical rail transportation vehicles. Combined with energy storage devices, WPT technology can promote the development of electric vehicles [4–6].

In some practical applications of WPT technology, there are various types of loads, such as battery, supercapacitor (SC), and electric motor [7–9]. In the application of rail transit vehicles, an SC is considered suitable as an on-board energy storage device, because of the following characteristics: (1) high power density; (2) accurate measurement of state of charge; (3) long cycle-life and low maintenance cost; and (4) lack of use of heavy-metal chemical materials and, thus, low environmental pollution [10,11]. With these advantages, SC can be chosen as a WPT system load for power supply. For such a WPT system applied in electric vehicles, a three-phase rectifier is used to convert the grid alternating current (AC) voltage to the direct current (DC) bus voltage. Typically, the transmitter is fed with a high frequency AC current which is converted via a single-phase inverter and generates an AC magnetic flux linkage; then, the receiver induces an AC current for supplying power to the load. As the SC load requires a small DC current ripple, a filter is typically connected between the AC/DC rectifier and SC, as shown in Figure 1. When the load and system parameters are designed reasonably and remain constant, a constant-load-resistance WPT system can easily work stably and effectively. However, the output voltage and power of such an SC-load WPT system will vary during charging under a constant charging current, which will lead to changes in the system characteristics. This is not favorable in terms of the efficient and stable operation of the system.

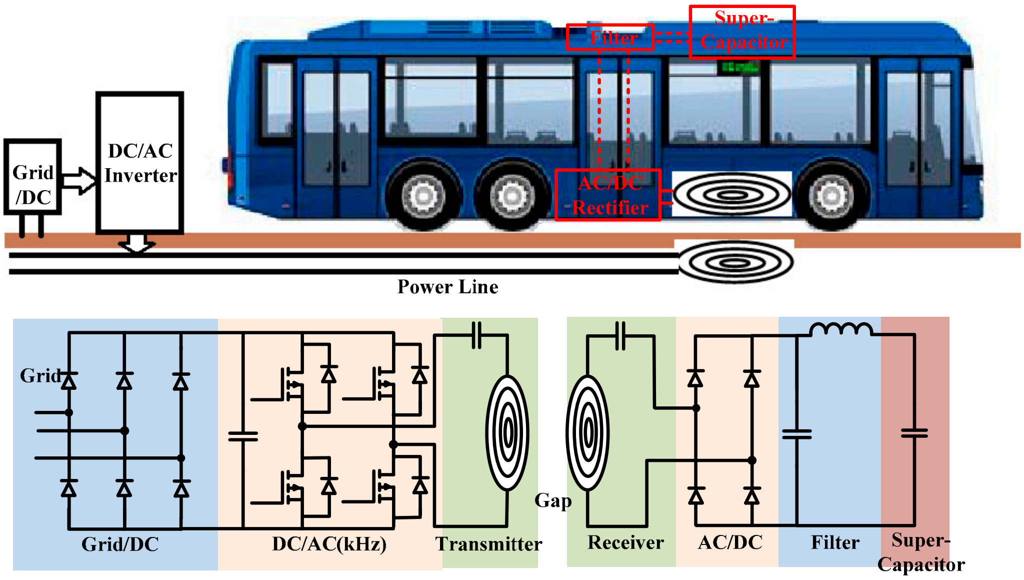

Figure 1. WPT system configuration in rail transit vehicle.

At present, the analysis of WPT systems is typically based on constant load resistance. The rectifier and load in the receiver side are generally considered as a constant load resistance [12–14]. Similarly, when studying only the variation of the coupling coils and system frequency, the change in load is rarely considered [15–17]. Furthermore, refs. [9,18] used a constant-voltage load model to analyze the battery load. These studies were based on the constant value of a load, which is not fully suitable for WPT systems which use the SC as the final load. The application of SC in a WPT system can be found in [19–24]. However, ref. [19] presents a technique for the suppression of voltage transients through use of dynamically reconfigurable SC banks, in which SC is not a load, but, instead, a parallel energy system. The authors of [20] considered an SC optimal control method in order to satisfy the requirements of efficiency and power; however, they did not analyze the charging characteristics. For the modeling and analysis of an SC-load WPT system, refs. [21,22] used a classical SC model as the WPT system load, but only established the relationship between the voltage, the current of the SC and the equivalent resistance of the WPT system, but did not consider the whole WPT system for analysis. The authors of [23,24] attempted to develop an SC as the WPT system load for relevant applications, but did not analyze system models. To solve the problem, the present paper proposes a variable-resistance-based (VRB) method which can describe the variation in the charging process of SCs. The analytical derivations and analysis could serve as a basis for developing WPT systems using SCs as on-board energy storage devices.

The remainder of this paper is organized as follows: In Section 2, the configuration of the SC-load WPT system is shown. A variable-resistance-based method is proposed for analyzing such a system, and the method is explained. The voltages and currents of the transmitter and receiver are derived according to the VRB method. In addition, the relationship between the output power and transfer efficiency with the voltage of an SC are calculated. In Section 3, the variations in the charging process with time are emphasized, including the voltage of an SC, the output power of the WPT system, and the transfer efficiency. The effect of the transmitter voltage on transfer efficiency is analyzed. Furthermore, the effects of frequency offset on the WPT system, including the effects on voltage gain and current gain, are studied, and then the design process for the SC-load WPT system is described. In Section 4, a simulation model and experimental platform are built to verify the theoretical analysis and calculation. Finally, the conclusions are drawn in Section 5.

2. WPT System Model Using SC Load

2.1. Variable-Resistance-Based WPT System Model

The topology of the SC-load WPT system in Figure 1 can be modeled by circuit theory, as shown in Figure 2. The system usually consists of a DC bus voltage, an inverter (working at tens of kHz), transmitting and receiving coils, a rectifier, a filter and an SC-load, where U_{bus} is the DC bus voltage, U_{SC} is the SC charging voltage, S1–S4 are the full-controlled semiconductor switches, D_1–D_4 are the diodes, R_1 (R_2), L_1 (L_2) and C_1 (C_2) are the transmitting (receiving) side coil resistance, inductance and series compensation capacitor, M is the mutual inductance of the transmitting and receiving side coils, C is an SC equivalent capacitor, C_d and L_d are a DC side filter capacitor and inductor, respectively, I_1 and I_2 are the root-mean-square (RMS) value of the transmitter current and the receiver current, respectively, and I_{SC} and U_{SC} are the RMS values of the SC charging current and voltage, respectively.

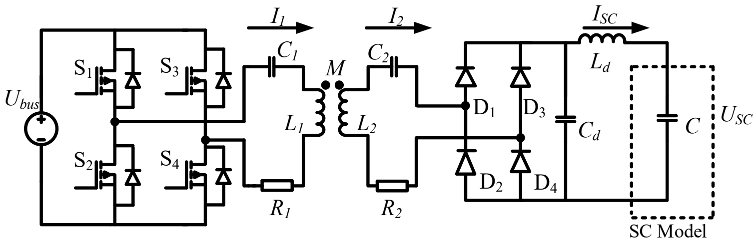

Figure 2. Topology of SC-load WPT system.

The full-bridge inverter transforms DC power into high-frequency AC power, and the receiving side rectifier converts AC power to DC power. Therefore, the AC voltages of the inverter and rectifier are square waves with amplitudes of U_{bus} and U_{SC}, respectively. According to the Fourier decomposition, only the fundamental frequency component is considered because the high-order harmonic components are so small, and these harmonics can hardly be transmitted. The equivalent circuit is demonstrated in Figure 3, where U_1 and U_2 are the fundamental RMS values of the AC side voltages of the inverter and the rectifier, I_1 and I_2 are the transmitter current and receiver current, and R_v is the equivalent resistance load for the receiving coil.

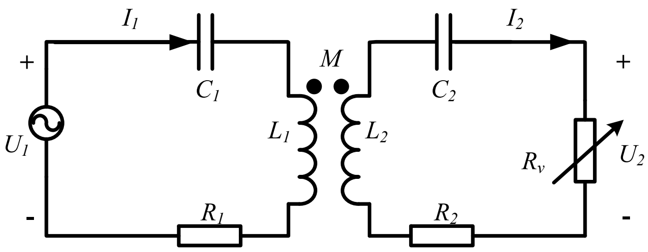

Figure 3. Equivalent circuit of VRB transmitter and receiver.

Based on the Fourier decomposition of the square wave, U_1 and U_2 are expressed as follows:

$$\begin{cases} U_1 = \frac{2\sqrt{2}}{\pi} U_{bus} \\ U_2 = \frac{2\sqrt{2}}{\pi} U_{SC} \end{cases} \tag{1}$$

Considering a WPT system charging for an SC with constant I_{SC}, and according to the characteristics of an SC, the terminal voltage will increase, which will lead to the equivalent resistance of SC varying, since its equivalent resistance R_{SC} can be defined as U_{SC} divided by I_{SC}. To consider the influence of using the SC as a load, the equivalent transformations of the rectifier and SC are adopted.

First, let the equivalent impedance seen by the receiver be a resistive load R_v, as shown in Figure 3. The key is to determine the relationship between the SC and R_v; this method is known as the variable-resistance-based method.

R_v can be calculated as:

$$R_v = \frac{U_2}{I_2} = \frac{8}{\pi^2}\frac{U_{SC}}{I_{SC}} \tag{2}$$

Based on the above description, the AC impedance method can be applied to approximately analyze the steady-state performance, as shown in Figure 3. According to Kirchhoff's voltage law (KVL), the transmitter and receiver voltages and currents in the equivalent circuit model are given as follows:

$$\begin{bmatrix} \dot{U}_1 \\ 0 \end{bmatrix} = \begin{bmatrix} Z_1 & -j\omega M \\ -j\omega M & Z_2 + R_v \end{bmatrix} \begin{bmatrix} \dot{I}_1 \\ \dot{I}_2 \end{bmatrix} \tag{3}$$

where ω is the real operating angular frequency, and Z_1 and Z_2 are the transmitter and receiver coil impedance, as follows:

$$\begin{cases} Z_1 = R_1 + j\omega L_1 + \frac{1}{j\omega C_1} \\ Z_2 = R_2 + j\omega L_2 + \frac{1}{j\omega C_2} \end{cases} \tag{4}$$

The I_1, I_2, output power (P_{OUT}) and transfer efficiency (η_{trn}) are solved as follows:

$$\begin{bmatrix} \dot{I}_1 \\ \dot{I}_2 \end{bmatrix} = \frac{1}{Z_1(Z_2 + R_v) + \omega^2 M^2} \begin{bmatrix} Z_2 + R_v & -j\omega M \\ -j\omega M & Z_1 \end{bmatrix} \begin{bmatrix} \dot{U}_1 \\ 0 \end{bmatrix} \tag{5}$$

$$P_{OUT} = U_2 I_2 \tag{6}$$

$$\eta_{trn} = \frac{U_2 I_2}{U_2 I_2 + I_1{}^2 R_1 + I_2{}^2 R_2} \tag{7}$$

2.2. Variable-Resistance Load Derivations

Typically, a transmitter and receiver are required under resonance to enhance the system transfer capability and efficiency. The compensation is a series-series method because the values of the compensation capacitor are not affected by load, and it is easily achieved. In addition, the series-series compensation has the characteristics of a constant output current, which is suitable for SC charging.

The resonant angular frequencies of the transmitter and receiver are obtained as follows:

$$\omega = \frac{1}{\sqrt{L_1 C_1}} = \frac{1}{\sqrt{L_2 C_2}} \tag{8}$$

In this case, Equation (5) can be simplified as follows:

$$\begin{bmatrix} \dot{I}_1 \\ \dot{I}_2 \end{bmatrix} = \frac{1}{R_1(R_2 + R_v) + \omega^2 M^2} \begin{bmatrix} R_2 + R_v & -j\omega M \\ -j\omega M & R_1 \end{bmatrix} \begin{bmatrix} \dot{U}_1 \\ 0 \end{bmatrix} \tag{9}$$

If the self-resistance of the coil is ignored, the I_2 is solved as follows:

$$I_2 = \frac{U_1}{\omega M} \tag{10}$$

It can be found that, if U_1, ω and M of the WPT system are all constant, I_2 can remain constant. Therefore, the SC charging current is also constant:

$$I_{SC} = \frac{2\sqrt{2}}{\pi}\frac{U_1}{\omega M} \tag{11}$$

In this case, U_{SC} can be calculated. Now u_{SC} is used to replace U_{SC}, because the voltage is varying at the process of charging; thus, u_{SC} can also be expressed as follows:

$$u_{SC} = \frac{I_{SC}}{C}t_{char} + U_{SC\_0} \tag{12}$$

where t_{char} is the charging time, and U_{SC_0} is the initial voltage of SC.

Substituting (11) into (12), u_{SC} can be rewritten as follows:

$$u_{SC} = \frac{2\sqrt{2}}{\pi}\frac{U_1}{\omega MC}t_{char} + U_{SC\_0} \tag{13}$$

Therefore, the charging current and voltage of the SC power supplied by the WPT system are determined. Furthermore, substituting (11) into (2), R_v can be simplified as follows:

$$R_v = \frac{2\sqrt{2}}{\pi}\frac{\omega M}{U_1}u_{SC} \tag{14}$$

R_v will change when u_{SC} increases; it is also determined by U_1, ω and M.

The power level of the system determines the choice of devices and the operating frequency ω of the system. Therefore, it is necessary to calculate and analyze the power level as follows:

$$P_{OUT} = \frac{2\sqrt{2}}{\pi}\frac{U_1}{\omega M}u_{SC} \tag{15}$$

As shown in Figure 3, the transfer efficiency is defined as the power consumed by R_v divided by the power generated by the source. Taking the transmitter and receiver power losses into consideration, the transfer efficiency is derived as follows:

$$\eta_{trn} = \frac{\omega^2 M^2 R_v}{R_1(R_2+R_v)^2 + \omega^2 M^2 (R_2+R_v)} \tag{16}$$

Considering the charging process of SC causing the variation of R_v, the efficiency of the WPT system using the SC as load can be obtained as follows:

$$\eta_{trn} = \frac{\omega^2 M^2 \frac{2\sqrt{2}}{\pi}\frac{\omega M}{U_1}u_{SC}}{R_1\left(R_2 + \frac{2\sqrt{2}}{\pi}\frac{\omega M}{U_1}u_{SC}\right)^2 + \omega^2 M^2\left(R_2 + \frac{2\sqrt{2}}{\pi}\frac{\omega M}{U_1}u_{SC}\right)} \tag{17}$$

Using the VRB method, it is easy to relate u_{SC} to the WTP system parameters.

3. Analysis of SC-Load WPT System

3.1. Variation in Charging Process with Time

In the process of charging for SC, R_v, u_{SC}, P_{OUT} and η_{trn} vary with the charging time. First, the charging time will cause a linear change of u_{SC} under the constant current. Then, R_v will increase linearly, which will result in I_1 changing, as shown in Equation (10). Next, U_2 will increase, then P_{OUT} will increase with the charging time. In practical conditions, the variations will occur at the same time. Based on the above deviations and analysis, the relationship between these key parameters is shown as Figure 4.

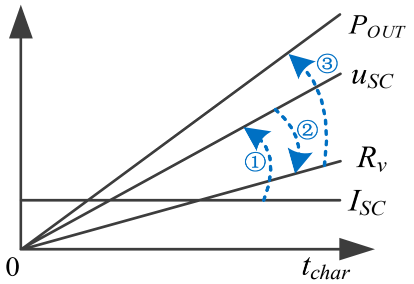

Figure 4. Relationship between some key parameters.

The SC voltage with charging time is shown as (13). Similarly, R_v and P_{OUT} with charging time are calculated as follows:

$$R_v = \frac{8}{\pi^2 C} t_{char} + \frac{2\sqrt{2}}{\pi} \frac{\omega M}{U_1} U_{SC-0} \tag{18}$$

$$P_{OUT} = \frac{2\sqrt{2}}{\pi} \frac{U_1}{\omega M} \left(\frac{2\sqrt{2}}{\pi} \frac{U_1}{\omega MC} t_{char} + U_{SC-0} \right) \tag{19}$$

In practical applications, especially in high-power applications, such as rail transportation, WPT system efficiency is particularly significant. A miniscule decline in efficiency will cause much energy loss. In addition, the transfer efficiency of the SC-load WPT system is different from other types of load and is variable over a wide range. This is why it is necessary to analyze the transfer efficiency, which is shown as (17), and the transfer efficiency is maximized when:

$$\frac{\partial \eta(u_{SC})}{\partial u_{SC}} = 0 \,\&\, \frac{\partial^2 \eta(u_{SC})}{\partial u_{SC}} < 0 \tag{20}$$

Then, the optimal value ($u_{SC\_OPT\_\eta}$) of u_{SC} can be solved as follows:

$$u_{SC\_OPT\_\eta} = \frac{\pi U_1 R_2}{2\sqrt{2} \omega M} \sqrt{1 + \frac{\omega^2 M^2}{R_1 R_2}} \tag{21}$$

The maximum transfer efficiency ($\eta_{trn\_\max}$) is derived as follows:

$$\eta_{trn\_\max} = \frac{\sqrt{1 + \frac{\omega^2 M^2}{R_1 R_2}}}{1 + \sqrt{1 + \frac{\omega^2 M^2}{R_1 R_2}} + \frac{R_1 R_2 \left(1 + \sqrt{1 + \frac{\omega^2 M^2}{R_1 R_2}}\right)^2}{\omega^2 M^2}} \tag{22}$$

The transfer coil quality factor (T_Q) [9] is defined as follows:

$$T_Q = \frac{\omega M}{\sqrt{R_1 R_2}} \tag{23}$$

Considering that T_Q varies from 10 to 400, the theoretical result is shown as Figure 5. It can be seen that higher T_Q is beneficial to $\eta_{trn\_\max}$. From (33), it can be seen that high ω, large M and small R_1/R_2 can improve the maximum transfer efficiency.

$$\eta_{trn\_\max} = \frac{\sqrt{1 + T_Q{}^2}}{1 + \sqrt{1 + T_Q{}^2} + \frac{\left(1 + \sqrt{1 + T_Q{}^2}\right)^2}{T_Q{}^2}} \tag{24}$$

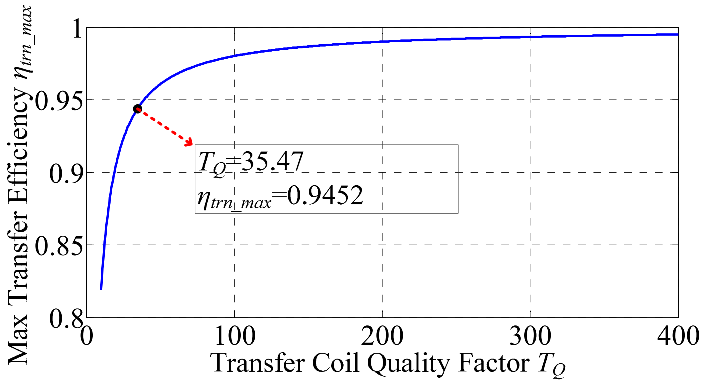

Figure 5. Curve of the maximum efficiency vs. T_Q.

The experimental prototype of the SC-load WPT system parameters are tabulated in Table 1. For this platform, its T_Q is equal to 35.47; thus, the maximum efficiency is about 0.9452. However, as discussed above, the efficiency will vary over a wide range. In addition, the variation in transfer efficiency must be analyzed. Substituting the system parameters into (17), the transfer efficiency vs. u_{SC} is plotted in Figure 6. When using the WPT system charging an SC, u_{SC} increases from 0 V to 100 V, and the transfer efficiency tends to rise, then fall. When u_{SC} is up to $u_{SC\_OPT\_\eta}$, η_{trn_max} can be obtained. Therefore, in practical applications, a suitable work voltage range of the SC should be chosen to obtain high efficiency.

Table 1. Experiment platform parameters.

Symbols	Note	Value
U_{bus}	DC bus voltage	80 V
f	Operating frequency	58 kHz
L_1	Transmitting side coil inductance	174.6 µH
L_2	Receiving side coil inductance	175 µH
R_1	Transmitting side coil self-resistance	0.23 Ω
R_2	Receiving side coil self-resistance	0.29 Ω
M	Mutual inductance	47 µH
C_1	Transmitting side compensation capacitance	44.4 nF
C_2	Receiving side compensation capacitance	44.2 nF
C	Load SC	18 F
L_d	Filter inductance	2.5 mH
C_d	Filter capacitance	500 µF

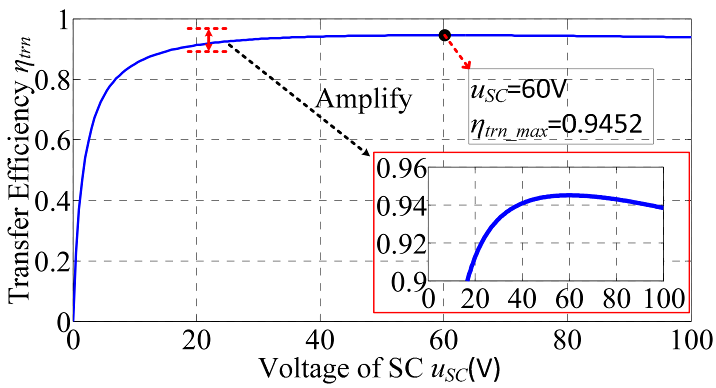

Figure 6. Curve of the transfer efficiency vs. u_{SC}.

3.2. Effects of Transmitter Voltage on Efficiency

According to Equation (17), if the coupling coil is designed well, based on (23), a high T_Q can enhance the transfer efficiency, and the transfer efficiency can be determined by U_1. In addition, U_1 is converted via an inverter. Typically, the phase-shift control is adopted to adjust U_1. According to the Fourier decomposition, the fundamental harmonic value of the transmitter voltage U_1 can be expressed as follows:

$$U_1 = \frac{2U_{bus}}{\pi}\sqrt{1+\cos\alpha} = \frac{2\sqrt{2}U_{bus}}{\pi}\cos\frac{\alpha}{2} \tag{25}$$

where α is the phase-shift angle.

Substituting Equation (25) into (17), the efficiency can be rewritten as follows:

$$\eta_{trn} = \frac{\frac{\omega^3 M^3}{U_{bus}\cos\frac{\alpha}{2}} u_{SC}}{R_1\left(R_2 + \frac{\omega M}{U_{bus}\cos\frac{\alpha}{2}} u_{SC}\right)^2 + \omega^2 M^2\left(R_2 + \frac{\omega M}{U_{bus}\cos\frac{\alpha}{2}} u_{SC}\right)} \tag{26}$$

If the transmitter and receiver are almost the same, R_1 is equal to R_2. Then, $u_{SC\_OPT\_\eta}$ can be rewritten as follows:

$$u_{SC\_OPT\_\eta} = U_{bus}\cos\frac{\alpha}{2} \tag{27}$$

First, only U_{bus} is considered, the phase-shift angle is assumed as zero, then (27) can be simplified as u_{SC_OPT} = U_{bus}. For such a WPT system, if we seek to maintain high efficiency, the work range of SC should be close to U_{bus}, or U_{bus} should be controlled to match the SC charging voltage.

Next, the effect of the diffident DC bus voltage on the transfer efficiency is considered. Letting U_{bus} of Equation (26) vary from 10 V to 100 V, the results are shown as Figure 7. When U_{bus} increases, the maximum transfer efficiency can be obtained when U_{bus} is the same as $u_{SC\_OPT\_\eta}$, as the red line shows. It can be found from the surface that, if the SC-load WPT system is intended to maintain a high transfer efficiency in the process of charging, then U_{bus} should be optimally designed. For example, based on the Table 1, if u_{SC} operates on 30 V to 50 V, a 40 V DC bus voltage can be chosen.

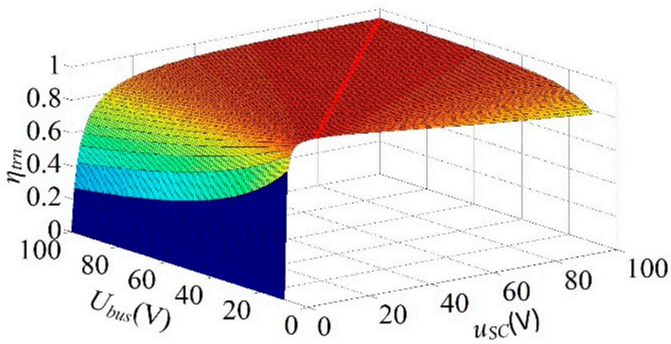

Figure 7. Transfer efficiency vs. U_{bus} and u_{SC}.

Then, the phase-shift angle requires to be considered. Assuming that U_{bus} is a constant 60 V and R_1 is equal to R_2, α is normally controlled in the range of 0° to 180°, and the radian is about 0–3, then the results obtained are those plotted in Figure 8. The results show that the transfer efficiency can be adjusted by the value of the phase-shift angle. When Equation (27) is satisfied, the maximum transfer efficiency can be obtained, as shown by the red line.

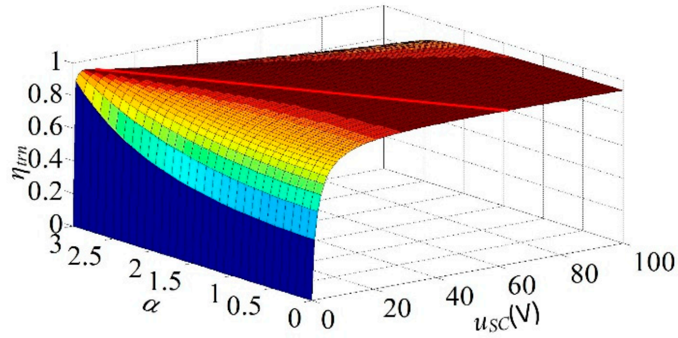

Figure 8. Transfer efficiency vs. α and u_{SC}.

The transmitter voltage is decided by both the DC bus voltage and the phase-shift angle, and these two factors further affect the transfer efficiency.

3.3. Effects of Frequency Offset on WPT System

In practical applications of the WPT system, the value of the compensation capacitor cannot be selected continuously, and the operating frequency may need to be adjusted to achieve the soft-switching of the inverter. Therefore, it is possible to cause the operating frequency to deviate from the resonant frequency, so it is necessary to analyze the effects of frequency offset on the SC-load WPT system.

The requirements for SC charging are constant current and fast charging. These can be satisfied under resonance, as shown in the above analysis. It is easy to determine how the frequency deviation will result in the receiver current varying from the R_v. Then I_{SC} cannot remain constant; thus, the characteristics of the SC-load WPT system will be different. Under the non-resonance of the transmitter and receiver, I_2 can be obtained according to (5), and I_{SC} can be calculated as follows:

$$I_{SC} = \frac{\frac{2\sqrt{2}}{\pi}\omega M U_1}{Z_1(Z_2 + R_v) + \omega^2 M^2} \tag{28}$$

It can be observed that I_{SC} will vary with the change in R_v, and that R_v is affected by I_{SC}. Therefore, the variation in R_v cannot be calculated as shown in (14). However, R_v can be calculated based on (2), by testing the voltage and current of SC, or by another calculation method, as shown below.

Assuming I_{SC} can remain constant at a slight time delay (t), the initial value of I_{SC} (I_{SC_0}) can be obtained from (28), when R_v = 0 and the initial SC voltage (u_{SC_0}) is zero. Therefore, the SC voltage (u_{SC_k}) and current (i_{SC_k}) at every moment can be calculated as follows:

$$\begin{cases} i_{SC\_k} = \dfrac{\frac{2\sqrt{2}}{\pi}\omega M U_1}{Z_1\left(Z_2 + \frac{8}{\pi^2}\frac{u_{SC\_k-1}}{i_{SC\_k-1}}\right) + \omega^2 M^2} \\ u_{SC\_k} = u_{SC\_k-1} + \dfrac{i_{SC\_k-1}}{C}\Delta t \end{cases} \tag{29}$$

where k represents the moment of SC charging.

Then the variable resistance R_v can be calculated as:

$$R_v = \frac{8}{\pi^2} R_{SC} = \frac{8}{\pi^2}\frac{u_{SC\_k}}{i_{SC\_k}} \tag{30}$$

R_v has two variables, u_{SC_k} and i_{SC_k}, compared with the constant charging current, which can be expressed as a variable u_{SC}. We can use a variable (R_{SC}) instead of two variables (u_{SC_k} and i_{SC_k}); then the characteristics of the SC-load WPT system under frequency deviation can be analyzed based on the VRB method, and the difference can be used simultaneously to measure the voltage and the current to determine the variable resistance R_v.

The voltage gain (G_V) refers to the ratio of the output voltage to the input voltage, so G_V can show the change in receiver voltage when U_1 is constant. The current gain (G_I) is analyzed similarly. The analysis below and calculation are based on the equivalent circuit model shown in Figure 3.

Here, the angular frequency offset (ω_n) is defined as the operating angular frequency (ω) divided by the resonant angular frequency (ω_n):

$$\omega_n = \frac{\omega}{\omega_0} \tag{31}$$

G_V is defined as:

$$G_V = \left|\frac{v_o}{v_i}\right| = \left|\frac{j\omega M R_L}{(Z_1 + Z_r)(Z_2 + R_v)}\right| \tag{32}$$

where $Z_r = \omega^2 M^2/(Z_2 + R_v)$. After ignoring the coil self-resistances, and substituting the parameters into (32), G_V can be obtained as:

$$G_V = \frac{j\omega^3 C_P C_S M R_L}{R_e + jI_m} \tag{33}$$

Considering the above formula, it can be further deduced as

$$G_V = \frac{nk{\omega_n}^3}{\sqrt{{\omega_n}^2(1-{\omega_n}^2)^2 + \left(\frac{\pi^2 i_{SC\_k}\omega_0 L_2}{8u_{SC\_k}}\right)^2\left((1-{\omega_n}^2)^2 - k^2{\omega_n}^4\right)^2}} \tag{34}$$

where $k = M/\sqrt{L_1 L_2}$ is the coupling coefficient of the transmitter and receiver coils, and $n = \sqrt{L_1/L_2}$ is the effective turn ratio of the transmitter and receiver coils.

Similarly, G_I can be calculated as follows

$$G_I = \frac{n{\omega_n}^2 k}{\sqrt{\left(\frac{8R_{SC}\omega_n}{\pi^2\omega_0 L_2}\right)^2 + (1-{\omega_n}^2)^2}} \tag{35}$$

Taking Table 1 into consideration, the results can be plotted as shown in Figures 9 and 10. At the point ω_n = 1, it is consistent with the above analysis. The voltage gain is a linear rise, and the U_2 and SC voltage will increase linearly if the U_1 is constant. However, if ω_n is shifted, G_I will decrease when R_{SC} is larger. In contrast, G_U will increase and have two peak points when R_{SC} is smaller, as shown in Figure 9.

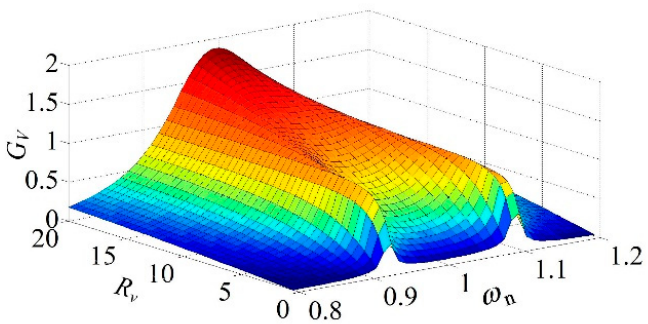

Figure 9. Voltage gain G_V vs. R_{SC} and ω_n.

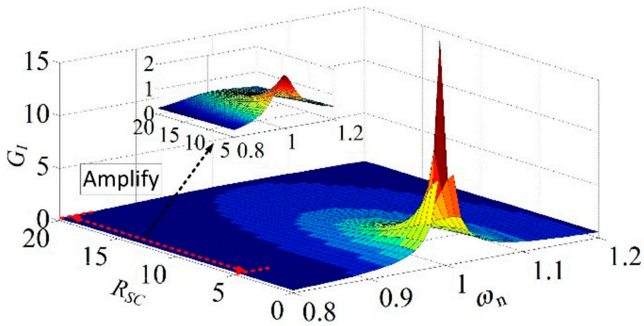

Figure 10. Current gain G_I vs. R_{SC} and ω_n.

As for the current gain shown in Figure 10, I_2 will remain constant, and I_1 will increase linearly under the resonant frequency; thus, the curve of G_I is an inverse proportion function when ω_n = 1. When the operating frequency is shifted, G_I will decrease, especially when R_{SC} is smaller. Based on this analysis, it can be concluded that a small R_{SC} is not favorable, and the system will demonstrate better characteristics when R_{SC} is chosen as the suitable value.

3.4. Design Process of SC-Load WPT System

Based on the above analysis, the characteristics of the SC load WPT system can be determined, and the optimal design method for the SC-load WPT system can be preliminarily given. First, the key parameters of the SC load need to be determined according to the application. Considering the constant current charging for the SC, and the range of the operating voltage and time of SC requirements, the capacitance value of the SC can be calculated. Furthermore, the parameters of the WPT system can be designed. According to the SC maximum charging power, the higher frequency of the switching devices is conducive to improving the transfer efficiency. Next, the DC bus voltage can be set suitably, and, if it is limited, the phase-shift angle can be designed according to (27). Then, the mutual inductance can be determined. Finally, the coupling coils should be designed to meet the requirements of the mutual inductance and achieve the smallest equivalent resistances of the transmitter and receiver coils. The design procedure is shown as Figure 11.

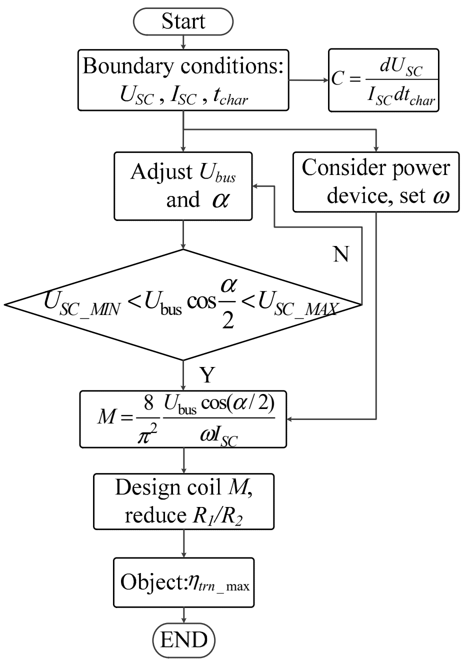

Figure 11. Design process.

4. Simulation and Experiment Verification

4.1. Simulation and Experimental Setup

To verify the theoretical derivations and analysis, an experimental prototype was fabricated as shown in Figure 12. The topology of the WPT system using SC as a load shared the same configuration with that in Figure 1. The parameters were consistent with Table 1. A SanRex three-phase bridge DF100AA160 was used to convert the grid AC to DC. A CREE SiC MOSFET C2M0080120D was adopted as the active switch of the inverter (DC/AC). Since the value of the compensation capacitor is limited, the inductance of the coupling coils is resonant with the compensation capacitor on the 58 kHz switching frequency. Therefore, this switching frequency was chosen as the system operating frequency. The transmitter and the receiver inductors were circular coils with a single layer and a turn number of 18, composed of tightly-wound litz wires with a diameter of 3 mm. The external diameter of the coil was 40 cm and the gap between the transmitter and receiver was 15 cm.

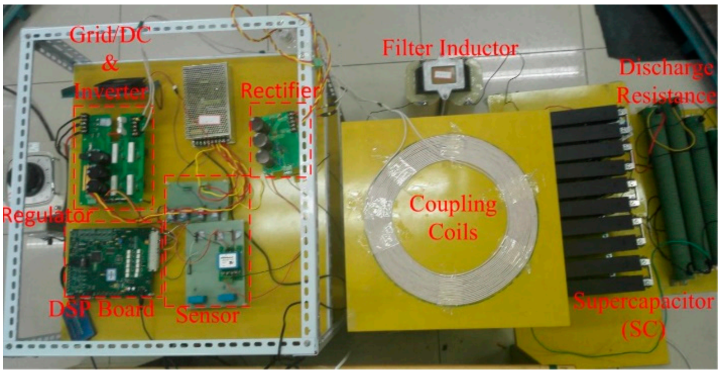

Figure 12. Demo SC-load WPT system.

The inductor and capacitor were chosen under the resonance for both the transmitter and receiver, and their resonant frequencies were the same as the operating frequency to improve the efficiency and reduce the VA rating of the WPT system. The SC voltage, charging current, transmitter and receiver AC currents and voltages were tested using a Tektronic DPO3034 digital phosphor oscilloscope. The series experiments were conducted in which the DC bus voltages were 40 V, 60 V and 80 V, respectively, with α = 45° under U_{bus} = 60 V, together with the corresponding simulations in PSIM, as displayed in Figure 13. For each series experiment, the SC was charged from non-energy (0 V) to 100 V under constant current charging.

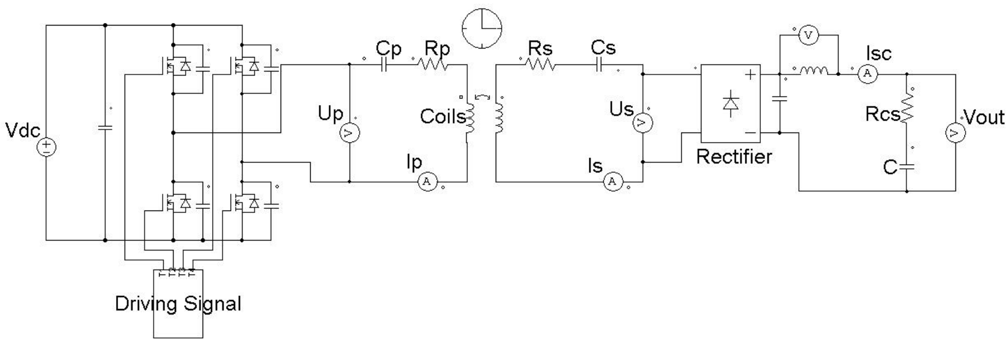

Figure 13. PSIM simulation model.

Under the 40 V DC bus voltage and phase-shift (0° and 45°), the recorded experimental waveforms of the transmitter input voltage (u_1), transmitter input current (i_1), receiver output voltage (u_2), and receiver output current (i_2) are shown in Figure 14.

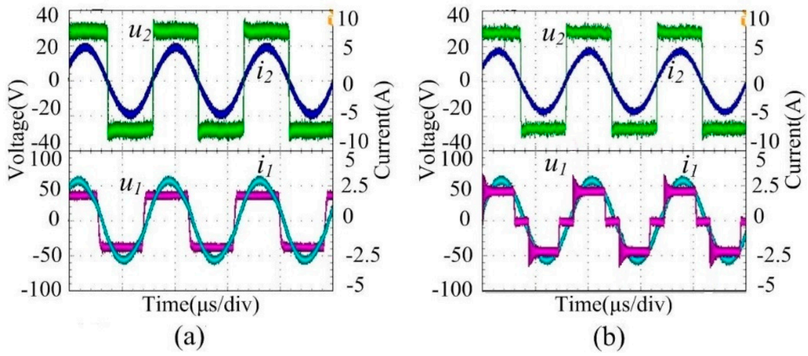

Figure 14. Experimental waveforms of u_1, i_1, u_2, i_2 (**a**) U_{bus} = 40 V & α = 0° and (**b**) U_{bus} = 40 V & α = 45°.

4.2. Results and Discussions

When using the WPT system charging for the SC from non-energy to 100V under a DC bus voltage of 60 V, the charging current and the output power are illustrated in Figure 15. The calculations of I_{SC} are constant, because the equivalent resistances of the transmitter and receiver (R_1 and R_2) are ignored. However, in the simulations and experiments, due to the existence of the R_1 and R_2, the charging current and output power decreased slightly, which was to be expected; thus, it can be concluded that the simulation and experimental results agree with the calculations, verifying the validation of the VRB method.

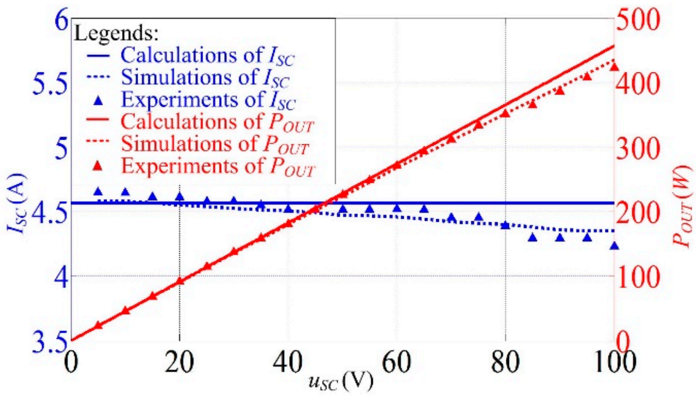

Figure 15. Calculations, simulations, and experiments of I_{SC}, P_{OUT}.

For adjustment of the DC bus voltages to 40 V, 60 V and 80 V, the calculations, simulations and experiments for transfer efficiency vs. u_{SC} are shown in Figure 16. The transfer efficiency η_{trn} increased then decreased, as in the analysis, and the maximum transfer efficiency point was where u_{SC} = U_{bus}. When U_{bus} increased, the corresponding optimal SC voltage increased, as shown in Figure 16a–c. The mismatches of the calculations, simulations and the experiments were generally caused by inaccuracy in the parameters. For U_{bus} = 60 V, the phase-shift angle was set at α = 45°, and u_{SC_OPT} was equal to 55 V, as shown in Figure 16d. The existence of the phase-shift angle resulted in the waveform of the transmitter U_1 distortion, as shown in Figure 14, and when u_{SC} increased the voltage shock increased. Due to the limitations of the experimental prototype, u_{SC} was only charged to 60 V, but it was verified that the optimal SC voltage dropped compared with α = 0°.

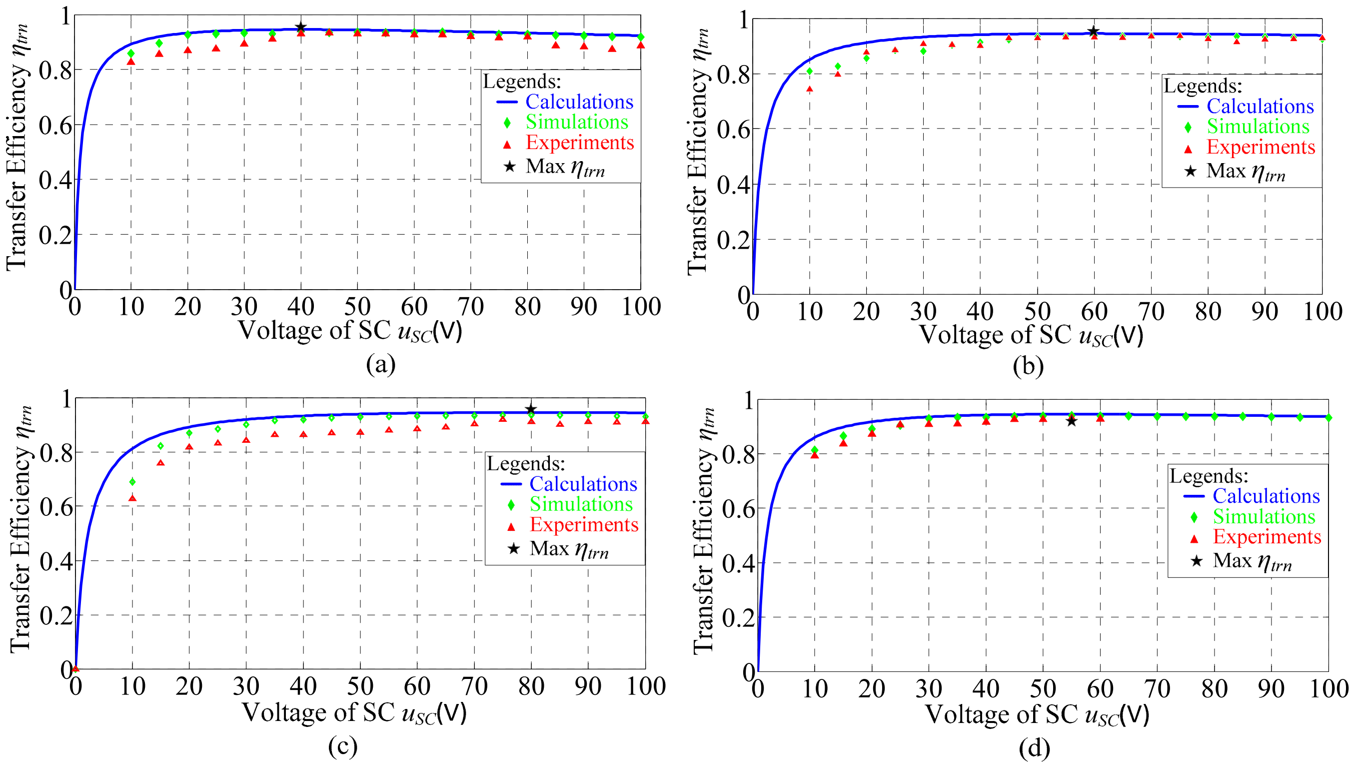

Figure 16. Curves of the transfer efficiency: (**a**) U_{BUS} = 40 V, α = 0°; (**b**) U_{BUS} = 60 V, α = 0°; (**c**) U_{BUS} = 80 V, α = 0°; (**d**) U_{BUS} = 60 V, α = 45°.

5. Conclusions

In existing WPT system model analysis methods, the equivalent resistance is often used to analyze various loads. For an SC load, the equivalent load will change in real time during the charging process, and the conventional model cannot accurately establish the relationship between the load and the system. To address this problem, a novel variable-resistance-based method was proposed to describe the relationship between the WPT system parameters (including equivalent load, output current, system power and transmission efficiency) and the SC parameters (including charging voltage, time and capacitance). Based on the method, a mathematical model of the WPT system using SC as a load was built. Additionally, the effects of the transmitter voltage on the transfer efficiency and the effects of frequency offset on the voltage and current gain were investigated. Based on the results, an optimal design process for the SC-load WPT system was provided to guide the system design. Finally, an experimental prototype and simulation model were constructed and the correctness of the theoretical analysis verified.

Author Contributions: Y.G. contributed significantly to analysis and manuscript preparation; T.W. contributed to the conception of the study; S.X. helped perform the analysis with constructive discussions; and Y.Y. provided experimental assistance. All authors have read and agreed to the published version of the manuscript.

Funding: This research was supported by the Scientific Research Foundation of Chongqing University of Technology (0107191157); This research was supported by the Science and Technology Research Program of Chongqing Municipal Education Commission (Grant No. KJQN202001145); This research was funded by the Natural Science Foundation of Chongqing, China, grant number cstc2021jcyj-msxmX0161.

Institutional Review Board Statement: Not applicable.

Informed Consent Statement: Not applicable.

Data Availability Statement: Not applicable.

Conflicts of Interest: The authors declare no conflict of interest.

References

1. Covic, G.A.; Boys, J.T. Modern trends in inductive power transfer for transportation applications. *IEEE J. Emerg. Sel. Top. Power Electron.* **2013**, *1*, 28–41. [CrossRef]
2. Trivio, A.; González-González, J.M.; Aguado, J.A. Wireless Power Transfer Technologies Applied to Electric Vehicles: A Review. *Energies* **2021**, *14*, 1547. [CrossRef]
3. Shin, J.; Shin, S.; Kim, Y.; Ahn, S.; Lee, S.; Jung, G.; Jeon, S.J.; Cho, D.H. Design and implementation of shaped magnetic-resonance-based wireless power transfer system for roadway-powered moving electric vehicles. *IEEE Trans. Power Electron.* **2014**, *61*, 1179–1192. [CrossRef]
4. Kim, J.H.; Lee, B.S.; Lee, J.H.; Lee, S.H.; Park, C.B.; Jung, S.M.; Lee, S.-G.; Yi, K.-P.; Baek, J. Development of 1-MW Inductive Power Transfer System for a High-Speed Train. *IEEE Trans. Ind. Electron.* **2015**, *62*, 6242–6250. [CrossRef]
5. Luo, B.; Long, T.; Guo, L.; Dai, R.; Mai, R.; He, Z. Analysis and Design of Inductive and Capacitive Hybrid Wireless Power Transfer System for Railway Application. *IEEE Trans. Ind. Appl.* **2020**, *56*, 3034–3042. [CrossRef]
6. Park, C.B.; Lee, H.-W. Study on the Optimal Switching Frequency for Maximum Wireless Power Transfer in a Variable Airgap System. *IEEE J. Emerg. Sel. Top. Power Electron.* **2015**, *3*, 201–204. [CrossRef]
7. Lee, G.; Kim, M.Y.; Lee, C.; Jang, D.; Lee, B.S.; Kim, J.H. Electromagnetic Field Tests of a 1-MW Wireless Power Transfer System for Light Rail Transit. *Energies* **2021**, *14*, 1171. [CrossRef]
8. Rossi, C. Design Procedure Based on Maximum Efficiency for Wireless Power Transfer Battery Chargers with Lightweight Vehicle Assembly. *Energies* **2021**, *15*, 70.
9. Zhang, Y.; Chen, K.; He, F.; Zhao, Z. Closed-form oriented modeling and analysis of wireless power transfer system with constant-voltage source and load. *IEEE Trans. Power Electron.* **2015**, *31*, 3472–3481. [CrossRef]
10. Mamun, A.A.; Liu, Z.; Rizzo, D.M.; Onori, S. An Integrated Design and Control Optimization Framework for Hybrid Military Vehicle Using Lithium-Ion Battery and Supercapacitor as Energy Storage Devices. *IEEE Trans. Transp. Electrif.* **2019**, *5*, 239–251. [CrossRef]
11. Wang, H.; Zhou, G.; Xue, R.; Lu, Y.; McCann, J.A. A Driving-Behavior-Based SoC Prediction Method for Light Urban Vehicles Powered by Supercapacitors. *IEEE Trans. Intell. Transp. Syst.* **2020**, *21*, 2090–2099. [CrossRef]
12. Choi, S.Y.; Huh, J.; Lee, W.Y.; Rim, C.T. Asymmetric coil sets for wireless stationary EV chargers with large lateral tolerance by dominant field analysis. *IEEE Trans. Power Electron.* **2014**, *29*, 6406–6420. [CrossRef]
13. Sample, A.P.; Meyer, D.A.; Smith, J.R. Analysis, experimental results, and range adaptation of magnetically coupled resonators for wireless power transfer. *IEEE Trans. Ind. Electron.* **2011**, *58*, 544–554. [CrossRef]
14. Wu, H.H.; Gilchrist, A.; Sealy, K.D.; Bronson, D. A high efficiency 5 kw inductive charger for EVs using dual side control. *IEEE Trans. Ind. Inform.* **2012**, *8*, 585–595. [CrossRef]
15. Imura, T.; Hori, Y. Maximizing air gap and efficiency of magnetic resonant coupling for wireless power transfer using equivalent circuit and Neumann formula. *IEEE Trans. Ind. Electron.* **2011**, *58*, 4746–4752. [CrossRef]
16. Kim, S.; Park, H.H.; Kim, J.; Kim, J.; Ahn, S. Design and analysis of a resonant reactive shield for a wireless power electric vehicle. *IEEE Trans. Microw. Theory Tech.* **2014**, *62*, 1057–1066. [CrossRef]
17. Zheng, C.; Ma, H.; Lai, J.S.; Zhang, L. Design considerations to reduce gap variation and misalignment effects for the inductive power transfer system. *IEEE Trans. Power Electron.* **2015**, *30*, 6108–6119. [CrossRef]
18. Neath, M.J.; Swain, A.K.; Madawala, U.K.; Thrimawithana, D.J. An optimal PID controller for a bidirectional inductive power transfer system using multi-objective genetic algorithm. *IEEE Trans. Power Electron.* **2014**, *29*, 1523–1531. [CrossRef]
19. Madawala, U.K.; Thrimawithana, D.J.; Kularatna, N. An ICPT-supercapacitor hybrid system for surge-free power transfer. *IEEE Trans. Ind. Electron.* **2008**, *54*, 3287–3297. [CrossRef]
20. Geng, Y.; Li, B.; Yang, Z.; Lin, F.; Sun, H. A high efficiency charging strategy for a supercapacitor using a wireless power transfer system based on inductor/capacitor/capacitor (LCC) compensation topology. *Energies* **2017**, *10*, 135. [CrossRef]
21. Li, Z.; Zhu, C.; Jiang, J.; Song, K.; Wei, G. A 3-kW Wireless Power Transfer System for Sightseeing Car Supercapacitor Charge. *IEEE Trans. Power Electron.* **2017**, *32*, 3301–3316. [CrossRef]
22. Wu, Y.; Zhang, C.; Liu, B. Research on the quick charging method of wireless power transfer system for supercapacitor. In Proceedings of the 2018 13th IEEE Conference on Industrial Electronics and Applications (ICIEA), Wuhan, China, 31 May–2 June 2018; pp. 582–587. [CrossRef]
23. Hanajiri, K.; Hata, K.; Imura, T.; Fujimoto, H. Maximum Efficiency Operation in Wider Output Power Range of Wireless In-Wheel Motor with Wheel-Side Supercapacitor. In Proceedings of the 44th Annual Conference of the IEEE Industrial Electronics Society (IECON 2018), Washington, DC, USA, 21–23 October 2018; pp. 5177–5182. [CrossRef]
24. Campagna, N.; Castiglia, V.; Miceli, R. Fuel Cell Based Inductive Power Transfer System for Supercapacitors Constant Current Charging. In Proceedings of the 2021 Sixteenth International Conference on Ecological Vehicles and Renewable Energies (EVER), Monte-Carlo, Monaco, 5–7 May 2021; pp. 1–6. [CrossRef]